Jurnal Tribologi 49 (2026) 68-82

MYTRIBOS Malaysian Tribology Society

Jurnal Tribologi

Website : jurnaltribologi.mytribos.org e-issn: 2289-7232

Hybrid thermochemical treatment effects on hardness and tribological behavior of LPBF-fabricated 316L stainless steel under dry and lubricated conditions

Nur Suraya Amad Mazni [1], Wardina Zalia Hariulnizam [1], Mohd Shahriman Adenan [1,2*], Minoru Goto [3]

[1] Smart Manufacturing Research Institute, Universiti Teknologi MARA, Jalan Ilmu 1/1, 40450 Shah Alam, MALAYSIA.
[2] Universiti Teknologi MARA, Faculty of Mechanical Engineering, Jalan ilmu 1/1, 40450 Shah Alam, MALAYSIA.
[3] Department of Mechanical Engineering, National Institute of Technology, Ube College, 2-14-1, Tokiwadai, 755-0097 Yamaguchi, JAPAN.
*Corresponding author: mshahriman@uitm.edu.my

KEYWORDS

316L stainless steel
Laser powder bed fusion
Hybrid thermochemical treatment
Tribological performance
DPBS lubrication

ABSTRACT

This study investigates hybrid thermochemical treatment applied to laser powder bed fusion (LPBF)-fabricated 316L stainless steel, aimed at enhancing surface hardness and wear resistance. The treatment was conducted in a tube furnace using a gas mixture of ammonia (NH_3), methane (CH_4) and nitrogen (N_2). Characterization was performed using X-ray diffraction (XRD) to detect the formation of the expanded austenite (S-phase) and scanning electron microscopy (SEM) for surface and subsurface microstructural evaluation. Mechanical performance was assessed by Vickers microhardness testing, while tribological behavior was evaluated under both dry and lubricated conditions using Dulbecco's phosphate-buffered saline (DPBS). The results indicate hybrid treatment produced more than double the surface hardness and significantly reduced the coefficient of friction compared to untreated LPBF 316L. These enhancements are attributed to the formation of a 12.2 µm-thick S-phase layer formed through simultaneous nitrogen and carbon diffusion. This study is the first to integrate hybrid diffusion with DPBS-based bio-tribological analysis for LPBF 316L offering potential for biomedical implants and high wear precision components.

Received 29 June 2025; received in revised form 8 October 2025; accepted 22 October 2025.
To cite this article: Amad Mazni et al. (2026). Hybrid thermochemical treatment effects on hardness and tribological behavior of LPBF-fabricated 316L stainless steel under dry and lubricated conditions. Jurnal Tribologi 49, pp.68-82.

1.0 INTRODUCTION

Austenitic stainless steels, particularly AISI 316L, are recognized for their superior corrosion resistance, leading to extensive use in demanding sectors such as aerospace, automotive, and medical devices (Cisquini et al., 2019). However, the fabrication of 316L traditionally relies on conventional methods such as casting and rolling, which cannot meet the demand for complex geometries and highly customized components. Additive manufacturing (AM) has emerged as a transformative technology, offering exceptional design flexibility, enabling customization, rapid prototyping and on-demand production while reducing material waste and tooling costs (Thompson et al., 2016; Alfaify et al., 2020; Hossain et al., 2024; Wang et al., 2024). The capabilities of AM vary depending on the specific technology used (Alfaify et al., 2020). Techniques such as laser powder bed fusion (LPBF) enable the fabrication of detailed and structured lattice designs, expanding possibilities in advanced manufacturing (Wang et al., 2024).

LPBF is widely recognized as a key metal additive manufacturing technique for producing complex engineering components (Sohif et al., 2025). In this process, a laser follows a bidirectional scanning strategy, with each line scanned in alternating directions and each layer rotated 90° to improve build quality. The design originates from slicing a 3D computer-aided design (CAD) model into thin, 2D cross-sections. A powder spreading system distributes a thin, even layer of metal powder over the build platform (Minasyan et al., 2020). However, defects may arise due to physical phenomena during laser-powder interaction, including unstable melt pool behavior, poor inter-particle bonding, material evaporation and the formation of unstable phases induced by rapid cooling rates (Tang et al., 2017; Ho et al., 2022).

Components fabricated using the LPBF method are often unsuitable in their as-built condition due to property deviations compared to conventionally manufactured counterparts. Rapid solidification and repeated thermal cycling during printing induce internal and residual stresses (Feng et al., 2024). Additionally, surface roughness and porosity defects formed during LPBF can degrade mechanical performance, including elastic and plastic deformation (Zhang et al., 2022), leading to reduced tribological performance under dry sliding conditions. These challenges necessitate surface modification strategies to enhance both hardness and wear resistance. Various post-processing approaches are employed, including laser surface treatment, mechanical finishing and thermochemical treatments (Mahmood et al., 2022). Among these, thermochemical treatments are particularly effective for enhancing 316L properties by forming a supersaturated S-phase (expanded austenite) layer, which improves surface hardness, wear, and corrosion resistance (Li et al., 2008; Zhang et al., 2022; Mahmood et al., 2022; Zhang et al., 2025).

The established surface treatments such as plasma and conventional thermochemical processes are widely used to overcome the limitations of 316L. (Li et al., 2008) studied the effects of plasma nitriding on 316L and reported the formation of a single S-phase with a thickness of approximately 6 μm. This treatment significantly increased surface hardness compared to untreated samples. However, plasma nitriding usually only affects the outer surface of a component, making it less suitable for complex shapes or parts with internal features. On the other hand, gas-based thermochemical treatments performed in tube furnaces allow better diffusion of nitrogen into both external and internal surfaces. (Zhang et al., 2025) demonstrated that thermochemical nitriding of 316L resulted in a thicker S-phase layer of about 19 μm, indicating better nitrogen penetration and improved surface properties compared to plasma treatment. As a result, thermochemical treatment is considered as more effective for components with complex or enclosed geometries such as those produced by the LPBF process. This enhancement on LPBF-fabricated 316L also offers a cost-effective alternative to expensive

materials like titanium or cobalt-chromium alloys (Feng et al., 2024). However, a single thermochemical treatment may not be enough for highly demanding applications. This is because it typically forms only a shallow diffusion layer with limited nitrogen or carbon content, which might not provide sufficient surface hardness and long-term durability. Nitrocarburizing and carbonitriding are examples of dual-layer treatments, which introduce nitrogen and carbon in separate stages and form two distinct layers with different properties (Jeyakymar et al., 2022; Xue et al., 2025) and have better enhancement compared to single-layer treatments.

In this study, an innovative hybrid thermochemical process was used. This method introduces both nitrogen and carbon simultaneously to the surface of LPBF 316L to improve its hardness and wear resistance. Unlike dual-layer treatments, the hybrid thermochemical treatment creates a single uniform layer with consistent surface characteristics. The hybrid treatment promotes the formation of an expanded austenite phase (γN and γC) also known as S-phase, which occurs when nitrogen and carbon atoms diffuse into the austenitic structure at low temperatures. These atoms distort the crystal lattice and generate compressive residual stresses that prevent dislocation movement which is an important mechanism for increasing hardness (Pinedo et al., 2011). The presence of S-phase layer significantly improves the resistance of LPBF 316L to wear and deformation under mechanical stress, addressing its typical weaknesses (Feng et al., 2024). In addition, S-phase layer contributes to a smoother surface and better load distribution, further improving the durability and service life of LPBF-fabricated components (Kong et al., 2020; Feng et al., 2024).

Previous studies by authors (Zainal et al., 2019; Azmi et al., 2022) have shown that hybrid thermochemical treatment on conventionally fabricated 316L can significantly improve the properties of conventionally manufactured 316L. Successful treatment depends on controlling parameters such as gas composition, treatment temperature, and holding time. However, the effects of the hybrid treatment on LPBF-fabricated 316L remain underexplored leaving an important research gap. Investigating these effects is crucial, as hybrid treatment could greatly enhance the surface properties and hardness of LPBF 316L. The aim of this study is to explore the microstructural evolution of LPBF 316L after hybrid thermochemical treatment. It also evaluates multiscale hardness performance, including Vickers microhardness and nanohardness indentation tests.

This study also introduces a novel approach by evaluating the tribological performance of 316L not only under dry conditions but also under lubricated conditions. While most previous studies have focused on using 316L for biomedical implants due to its excellent biocompatibility, where wear behavior is typically investigated only under dry sliding conditions. There remains limited work that simulates the lubricated environment of synovial joints in the human body (Chabak et al., 2021; Juri et al., 2023). This presents a gap in understanding how the enhanced surface properties of LPBF-fabricated 316L treated via hybrid process influence the tribological behavior under lubricated conditions Therefore, this study employed Dulbecco's phosphate-buffered saline (DPBS) as a lubricant to study the effect of lubricated conditions on hybrid-treated LPBF 316L.

2.0 EXPERIMENTAL PROCEDURE

2.1 Materials and Specimens Preparation

AISI 316L austenitic stainless steel (316L) was selected as the base material for specimen fabrication in this study. Two disc-shaped 316L specimens, each measuring 25 mm in diameter and 8 mm in thickness, were fabricated via LPBF process. The specimens were produced using gas-atomized 316L powder supplied by Renishaw Plc (UK), with the chemical composition presented in Table 1. The LPBF process was carried out using a Renishaw AM500 system equipped with a 500 W fiber laser. The key parameters included a laser power of 200 W, a scan speed of 1,200 mm/s, a layer thickness of 40 µm, and hatch spacing of 60 µm, as shown in Figure 1. Following fabrication, the specimens underwent stress relief at 330 °C for 3 hours under an inert atmosphere, in accordance with Renishaw AM500 SLM guidelines, to reduce residual stresses introduced during the process. Among the LPBF specimens, one was left untreated (designated as LPBF-U), while the other one was subjected to hybrid thermochemical surface treatments (designated as LPBF-H).

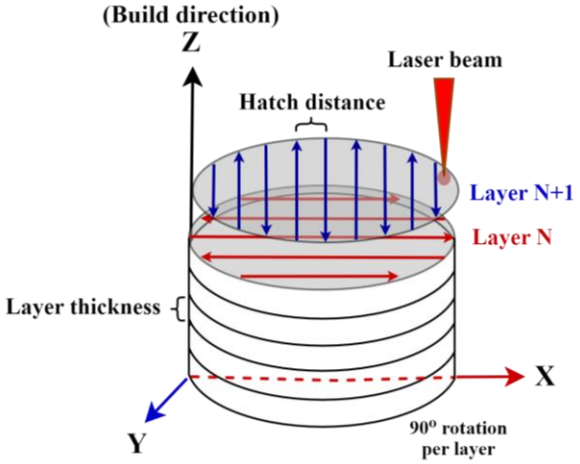

Figure 1: Schematic of the LPBF printing strategy

Table 1: Chemical composition (wt%) of 316L powder used in LPBF fabrication process (Renishaw, 2024).

Cr	Ni	Mo	Mn	Si	P	C	S	Fe
16-18	10-14	2-3	≤ 2	≤ 1	≤ 0.05	≤ 0.03	≤ 0.03	Bal.

2.2 Hybrid Thermochemical Treatment Process

Initially, the surface of the specimens underwent preparation to achieve mirror finish. This involved hot mounting in conductive resin, sequential wet grinding using silicon carbide (SiC) abrasive papers ranging from 240 to 1200 grit, followed by final polish with 0.03 µm of colloidal silica suspension. Before starting the heat treatment process, the specimens underwent a chemical cleaning step by immersing in a 2.0 M hydrochloric acid (HCl) solution for 15 seconds to eliminate the passive surface layer facilitating the treatment process.

The low-temperature hybrid thermochemical treatment process was then carried out using a customized gaseous tube furnace setup at temperature of 475 °C for 10 hours. The hybrid treatment was performed using a gaseous environment consisting of 15% nitrogen (N_2), 75% ammonia (NH_3), and 10% methane (CH_4), simultaneously introducing both nitrogen and carbon species into the specimen surface. NH_3 and CH_4 were utilized as the primary sources of nitrogen and carbon atoms, respectively while N_2 acted as the carrier gas. Before entering the tube furnace, the gaseous were channeled into a mixing chamber to ensure homogenous mixing with flow rate of 15 liters per minute. Figure 2 presents a schematic illustration of the experimental setup.

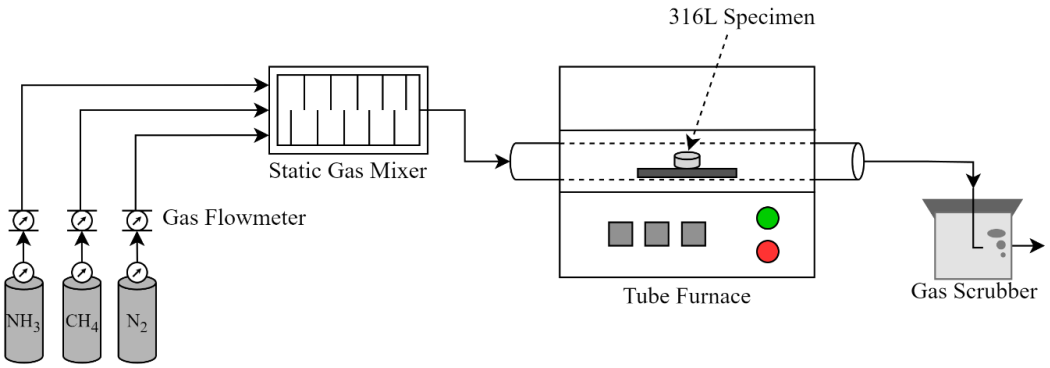

Figure 2: Schematic diagram of hybrid thermochemical treatment experimental setup.

2.3 Phase Identification and Microstructural Characterization

The characterization techniques employed in this study aimed to assess the formation of S-phase layer following the hybrid thermochemical treatment process. XRD analysis was conducted using a Rigaku Ultima IV diffractometer equipped with Cu-Kα radiation (λ = 1.5406 Å), operating at 40 kV and 40 mA. Scans were conducted over a 2θ range of 30° to 120°, with a step size of 0.02° and a scan speed of 2°/min. This method allows for precise phase identification and detection of lattice expansions indicative of S-phase formation. Furthermore, high-resolution imaging was conducted using Hitachi S-4300 scanning electron microscopy (SEM) to observe layer thickness, grain boundary evolution, and potential microcrack formation. Before SEM analysis, specimens underwent preparation through a standard grinding and polishing procedure, followed by etching with Kalling's Reagent No. 2 to enhance the visibility of the S-phase layer and reveal finer structural details.

2.4 Hardness Property Evaluation

Microhardness measurements were carried out on the specimen cross-sections using a Mitutoyo Vickers hardness tester (model MVK-H), following ASTM E384 guidelines. All tests were performed with a load of 200 gf and a dwell time of 10 seconds. To obtain the hardness profile from the top surface down to the substrate, three indentations measurements were taken directly on the specimen top surface (designated as 0 µm depth) to capture the maximum surface hardness of the treated layer. The mean values and standard deviations were calculated for the three indentations to ensure measurement reliability. Meanwhile, for cross-sections, six indentations were made at intervals of 0.05 to 0.50 mm from the surface to evaluate the hardness gradient.

2.5 Tribological Testing

The tribological properties were assessed using a ball-on-plate linear reciprocating tribometer under both dry and DPBS-lubricated sliding conditions at room temperature (25 ± 2 °C) and 50–60% relative humidity, following the ASTM G99-05 standard with modifications for a lower load. The system features a 3/16" steel ball bearing attached to a stationary pin, which is mounted on a lever arm that applies the load, while the specimen is positioned on a reciprocating disk. A normal load of 1 N was applied, with a sliding speed of 10 mm/s and a stroke length of 10 mm. Each test lasted for 60 minutes, and every condition was repeated three times to ensure repeatability and statistical relevance. Throughout the test, friction signals were recorded via wave logger system for real-data acquisition.

The dry conditions were conducted to simulate unlubricated contact scenarios, which are relevant to applications where lubrication is absent or minimal, such as in precision instruments and biomedical tools. The dry condition helps evaluate the fundamental wear behavior and surface durability of the material under direct asperity contact and moderate loading. For the investigation of lubricated conditions between the two sliding contact surfaces, 100 ml of pure DPBS (Nacalai Tesque, Inc. 14249-95) was used. This solution is sterile-filtered, free of calcium and magnesium, and has a pH of approximately 7.2. It contains typical isotonic salt concentrations such as 137 mM sodium chloride, 2.7 mM potassium chloride, 1.5 mM monobasic potassium phosphate, and 8.1 mM dibasic sodium phosphate. This artificial solution is commonly used to simulate the lubricating functions of natural body fluids in biomedical studies, particularly to assess the performance of 316L in applications that mimic human joint environments such as knee or hip implants (Rufaqua et al., 2021). A schematic diagram illustrating the lubricated condition of the wear is presented in Figure 3.

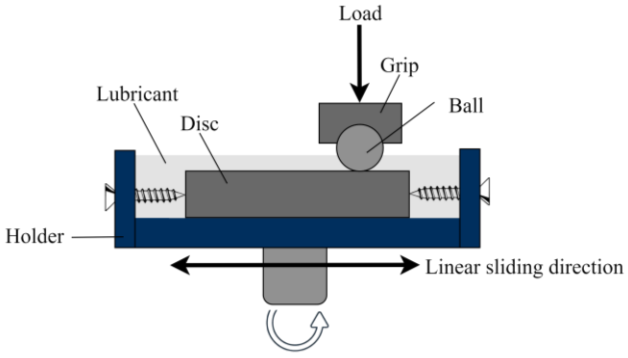

Figure 3: Schematic diagram illustrating ball-on-disk test in DPBS-lubricated condition.

3.0 RESULTS AND DISCUSSION

3.1 Formation of S-phase layer by thermochemical treatments

Analyzing XRD patterns is crucial to verify the effectiveness of the hybrid thermochemical treatment used in this study. Figure 4 illustrates XRD patterns obtained from both untreated and hybrid-treated 316L specimens. Compared to the untreated specimens, LPBF-H specimen exhibited broadened diffraction peaks and shifted towards lower 2θ angle, indicating lattice expansion due to nitrogen and carbon interstitial incorporation (Azmi et al., 2022). The γ (111)

peak at 43.55° in the LPBF-U specimen broadened and shifted to γN (111) at 39.7° in the LPBF-H specimen. A similar broadening and shift were observed in the γ (200) peak, which migrated to γC (200) at 45.5°, from its initial position at 50.6° in the LPBF-U specimen. These peak broadening and shifts toward lower 2θ angles confirming the formation of a supersaturated austenitic phase (S-phase) enriched with nitrogen and carbon. Both observed patterns of the peaks confirm the formation of S-phase layer resulting from the thermochemical treatment process (Shahriman et al., 2014; Zainal et al., 2019). The absence of chromium precipitation in the treated specimens further supports the successful and stable formation of the S-phase layer.

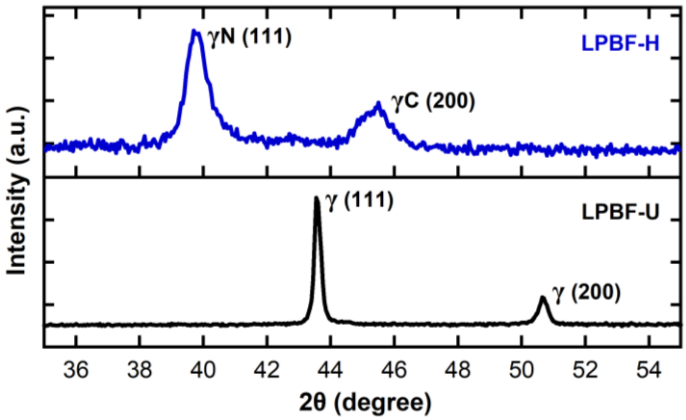

Figure 4: XRD diffractograms of LPBF-U and LPBF-H specimens, showing peak shifts and broadening due to thermochemical surface treatment.

The formation of the S-phase layer can be clearly observed from the SEM morphological analysis. The surface morphology observed in this study is consistent with previous findings (Shahriman et al., 2014; Zainal et al., 2019; Azmi et al., 2022), where the S-phase layer appeared as a uniform and homogenous bright region under SEM analysis, indicating effective layer formation and good corrosion resistance. Figure 5 shows the surface layer morphology of both specimens, where the LPBF-H developed a significantly thick S-phase layer, enriched with both nitrogen and carbon interstitial atoms, measuring an average thickness of 12.2 µm. The hybrid treatment in this study was conducted at 475°C for 10 hours and produced a thicker S-phase layer compared to those reported in previous studies using conventionally manufactured 316L. A study by Zainal et al., 2019 applied the same temperature and gas composition for 6 and 12 hours, producing S-phase layers of 6.85 µm and 8.05 µm, respectively. Despite the shorter holding time used in this study, the treatment exhibited a significantly thicker layer of 12.2 µm. This finding suggests that, even with a shorter treatment time, it was sufficient to promote the formation of a much thicker S-phase layer.

It should also be noted that the LPBF-H micrograph appears coarser and more porous compared to the LPBF-U specimen. This contrast mainly due to the etching process applied only to the LPBF-H specimen to reveal the formation of S-phase layer, whereas the LPBF-U specimen was left unetched. This difference in specimen preparation highlights microstructural features more prominently in LPBF-H but does not indicate actual porosity growth or microstructural degradation cause by the heat treatment. Similar observations have been reported in LPBF 316L studies by (Krakhmalev et al., 2018; Chabak et al., 2021). Additionally, microcracks were observed

in Figure 5(b) along the interface between the specimen and the resin mount. These cracks are attributed to mechanical loading during preparation process and are not expected to affect the performance of the material, as also supported by (Kurdi et al., 2024). Clear grain boundaries and a defined transition zone were observed in the cross-sectional surface of LPBF-H.

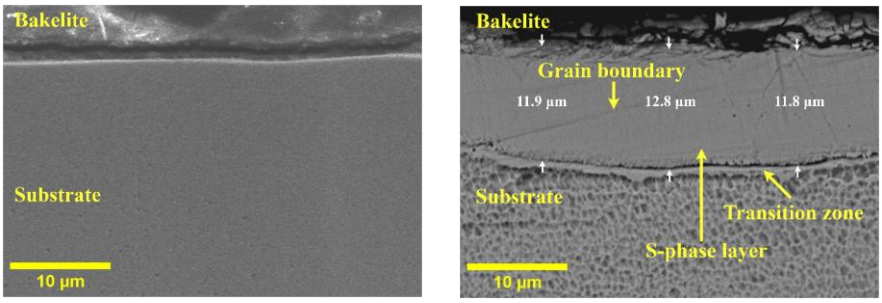

(a) (b)

Figure 5: Layer morphology of (a) LPBF-U and (b) LPBF-H specimens.

3.2 Effect of Thermochemical Treatments in Microhardness Properties

A microhardness test was performed on the cross-sectional area of the specimens using a 200 gf load to assess the distribution hardness within the specimen. As illustrated in Figure 6, the LPBF-U specimen exhibits a relatively uniform and lower hardness profile, with a maximum of approximately 264 HV and an average hardness of 254.05 ± 2.6 HV, consistent with the expected hardness of as-printed LPBF without surface treatment. In contrast, the LPBF-H specimen shows a significant surface hardening effect, reaching a peak hardness of ~1,209 ± 12.2 within the S-phase region. This is followed by a sharp reduction in hardness within the first 50 µm, after which the hardness stabilizes at an average value of 279.7 ± 3.5 HV deeper into the substrate.

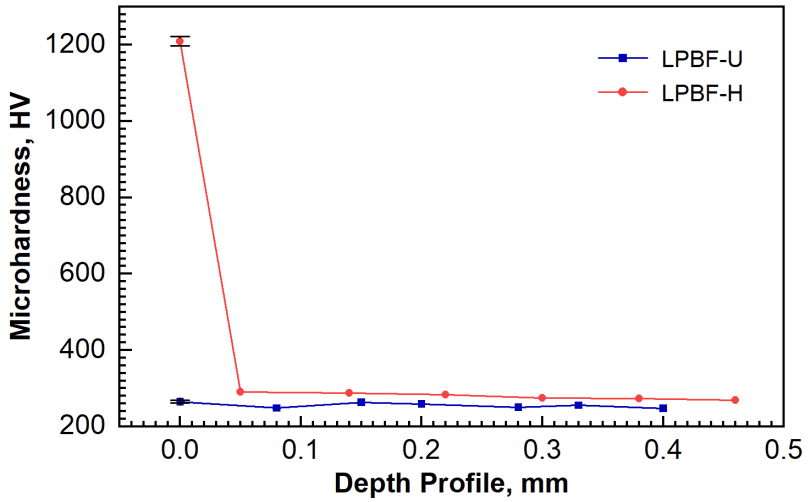

Figure 6: Microhardness profiles from the top surface down to the substrate of the LPBF-U and LPBF-H specimens.

Figure 7 clearly shows the indentation marks on top surface and cross-sectional areas from the microhardness tests. This hardness profile reflects the diffusion depth of nitrogen and carbon into the matrix, combined with the refined grain structure inherent to LPBF fabrication and confirms that the hardened S-phase region at the surface is responsible for the elevated surface hardness. The indentation marks in Figures 7(a) and 7(b) corroborate the top surface hardness values at 0 μm depth presented in Figure 6. The LPBF-U specimen displayed relatively large indentations, whereas the LPBF-H specimen shows markedly smaller indentation marks, as highlighted by the arrows in Figure 7(b). These results clearly indicate that the LPBF-H specimen exhibits significantly higher hardness compared to the untreated specimen.

A study by (Lopez et al., 2022) on 316L treated via nitrocarburizing reported a peak surface hardness of approximately 700 HV, which is much lower than the hardness achieved in the present hybrid-treated LPBF 316L. This shows the superior efficacy of the hybrid treatment applied in this study, where the selected parameters of 475 °C for 10 hours (Zainal et al., 2019), allowed nitrogen and carbon atoms to diffuse well into face-centered cubic (FCC) lattice without the precipitation of chromium nitrides or carbides, as also confirmed by Figure 4.

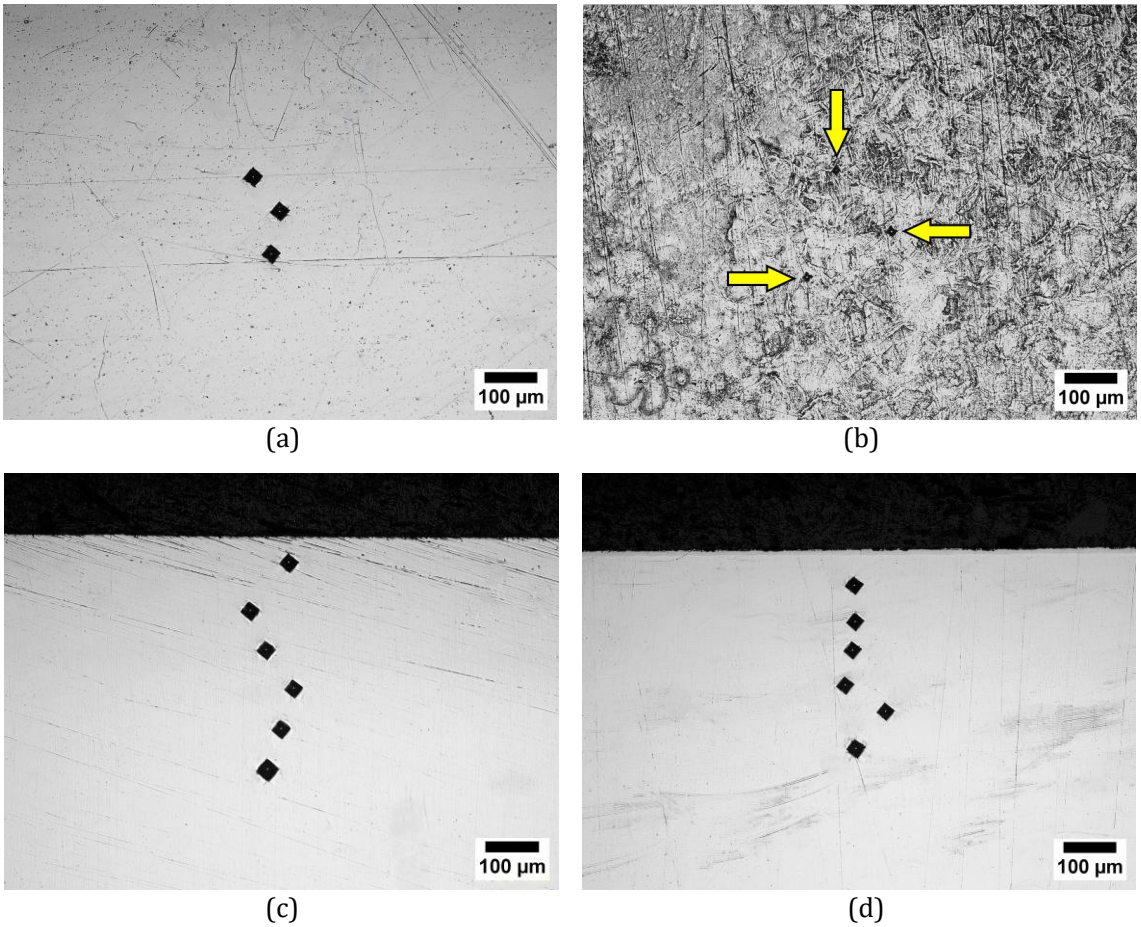

(a) (b)

(c) (d)

Figure 7: Indentation marks of (a) top surface LPBF-U, top surface LPBF-H, cross-sectional LPBF-U and cross-sectional LPBF-H specimens.

3.3 Wear and Frictional Performance

The surface integrity of LPBF 316L specimens were assessed using a ball-on-disk test under dry and DPBS-lubricated conditions with constant parameters such as sliding speed, applied load, and duration. Figure 8 presents the detailed wear morphology of specimens after subjected to the sliding conditions. Under dry sliding conditions, the observation revealed that LPBF-U specimen exhibited severe abrasive wear mechanisms, evidenced by the presence of deep grooves aligned with the sliding direction. These grooves are indicative of third-body abrasion, likely caused by hard wear debris formed through repeated adhesive interactions and surface fragmentation, as supported by the SEM images in Figure 8 and consistent with mechanisms (Elhadi et al., 2016; Aghababaei, 2019). In contrast, the LPBF-H specimen produced a reduced debris accumulation, with minimal wear debris. The smooth surface morphology observed in SEM for LPBF-H suggests a significant reduction in third-body abrasion, likely due to the integrity of the S-phase layer, as also reported in surface-treated stainless steel studies (Shahriman et al., 2014; Zainal et al., 2019; Azmi et al., 2022). This improved surface integrity is consistent with the higher surface hardness and the refined microstructure of LPBF 316L. As a result, the treated surface resists fragmentation, which reduces the generation of hard particles that typically act as abrasives and becomes more resistant to plastic deformation and abrasive wear during sliding contact (Elhadi et al., 2016).

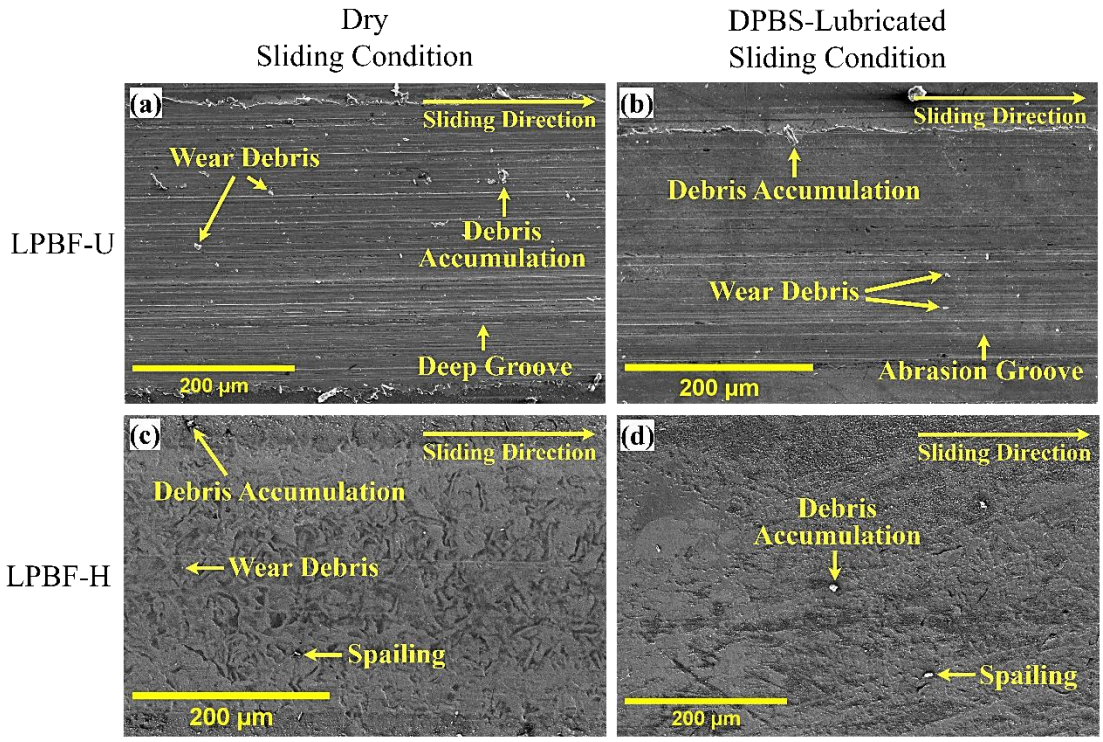

Figure 8: SEM images of the worn surfaces on 316L specimens under different thermochemical treatment and sliding conditions of (a) LPBF-U under dry sliding (b) LPBF-U under DPBS lubrication (c) LPBF-H under dry sliding and (d) LPBF-H under DPBS lubrication.

When tested under DPBS-lubricated conditions, both LPBF-U and LPBF-H specimens demonstrated improved wear behavior compared to dry sliding. The presence of DPBS reduced direct metal-to-metal contact, resulting in shallower wear tracks and less surface damage (Manhabosco et al., 2009; Wu et al., 2016). For LPBF-U, abrasion grooves and debris accumulation remained visible but were comparatively reduced. The reduction in wear track width suggests that the DPBS solution provided partial lubrication, limiting the severity of third body abrasion. In addition, the presence of DPBS may contribute to the formation of a protective tribochemical film, thereby preserving surface integrity (Shen et al., 2021; Chang et al., 2023; Chen et al., 2025). Meanwhile, the LPBF-H specimen exhibited the smoothest wear track, with minimal surface deformation and an absence of visible abrasion grooves. This can be attributed to the combined effect of a hardened surface from the formation of S-phase layer and effective DPBS lubrication. However, signs of localized spalling were observed on the LPBF-H under both dry and lubricated conditions. This surface delamination may be associated with subsurface crack initiation in the hardened S-phase layer as suggested by features observed in Figure 5.

Figure 9 shows the frictional performance of the specimens where the COF value was influenced by both surface treatment and sliding conditions. Under dry conditions, the LPBF-U specimen recorded the highest average COF (~0.95), with a gradually increasing trend throughout the test. The behavior reflects the severe abrasive wear observed in SEM, where repeated sliding caused the generation of hard debris and leads to increased friction due to repeated asperity interaction and debris accumulation on the worn surface (Wu et al., 2015). In contrast, the LPBF-H specimen showed a much lower and more stable average COF (~0.55) under dry conditions, suggesting improved wear resistance due to the presence of the S-phase layer, which enhances surface hardness and reduces material removal (Shahriman et al., 2014; Zainal et al., 2019), as shown in Figure 8. This improved resistance leads to a more stable sliding interface and significant friction reduction. This behavior highlights the strong link between hardness, microstructural refinement, and frictional stability. The hardened S-phase layer and refined grain structure reduces asperity interaction and limits the generation of wear debris, which collectively contributes to the lower and more stable COF values observed.

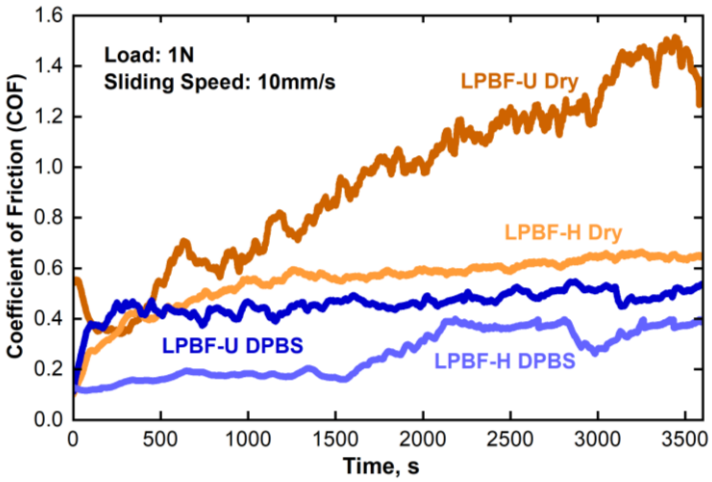

Figure 9: COF comparison of LPBF-U and LPBF-H specimens under both dry and DPBS-lubricated sliding conditions.

When tested under DPBS-lubricated conditions, both LPBF-U and LPBF-H specimens demonstrated significantly reduced average COF values compared to dry conditions, recorded at approximately ~0.46 and ~0.26, respectively. For LPBF-U, the drop in COF correlates with the fewer abrasion grooves and narrower track seen from the SEM morphology in Figure 8. Although not directly validated in this study, the reduction in COF may be partly attributed to the possible formation of a tribochemical film at the contact interface (Chen et al., 2025). Meanwhile, the LPBF-H specimen under DPBS showed the lowest and most stable COF throughout the test. This corresponds with the smoothest wear morphology observed in SEM with minimal deformation. The hardened surface from S-phase formation with the lubricating of DPBS effectively minimized metal-to-metal contact, thus improving the wear and friction performance (Qi et al., 2022; Ibrahim et al., 2025). However, a slight increase was observed after 1500 seconds, possibly due to evolving surface conditions such as tribochemical film disruption or localized changes in S-phase integrity under DPBS-lubricated sliding. Early in the test, DPBS likely forms a boundary film that effectively lowers friction and protects the surface. As sliding continued, this film may be worn away or chemically altered, leading to increased metal-to-metal interaction and thus slightly higher COF values (Elhadi et al., 2016; Rahmatian et al., 2023; Azizan et al., 2025).

4.0 CONCLUSION

This study assessed the surface characteristics and tribological performance of LPBF 316L subjected to hybrid thermochemical treatment. XRD analysis confirmed the formation of a supersaturated S-phase layer, evidenced by peak broadening and a shift to lower 2θ angles. The enrichment of nitrogen and carbon expanded the FCC lattice, which substantially increased hardness and improved anti-wear behavior under both dry and DPBS-lubricated conditions. Ball-on-disk tests showed smoother tracks, reduced debris formation, and lower average COF values for the treated specimens compared to the untreated-LPBF 316L. These improvements are primarily attributed to the hardened S-phase layer acting as a protective barrier during sliding.

This work highlights the potential of hybrid thermochemical treatment to extend the service life of LPBF 316L components in both dry and lubricated environments, where high corrosion resistance, superior surface hardness, and excellent wear performance are required. However, this study was limited to a single load and sliding speed hence, future work should explore a wider range of parameters, as well as long-term corrosion and wear interactions, to fully validate the treatment's effectiveness under diverse service conditions.

ACKNOWLEDGEMENT

The authors gratefully acknowledge the financial support from the Japan Student Services Organization (JASSO).

REFERENCES

Adenan, M. S., Berhan, M. N., & Haruman, E. (2014). Formation of expanded austenite using hybrid low temperature thermochemical heat treatment on 2205 duplex stainless steel. Advanced Materials Research, 970, 244-247.

Adenan, M. S., Zainal, S. U., & Haruman, E. (2019). S-phase layer development on 316 LVM using low temperature hybrid thermochemical treatment process. International Journal of Engineering and Advanced Technology, 9, 5845-5849.

Aghababaei, R. (2019). Effect of adhesion on material removal during adhesive wear. Physical Review Materials, 3(6), 063604.

Alfaify, A., Saleh, M., Abdullah, F. M., & Al-Ahmari, A. M. (2020). Design for additive manufacturing: A systematic review. Sustainability, 12(19), 7936.

Azizan, M. A. H., Sulaiman, M. H., & Yaakob, Y. (2025). Influence of propylene glycol on the tribological performance and lubrication mechanism of water-based lubricants incorporating silicon carbide, magnesium oxide and aluminium oxide nanoadditives. Jurnal Tribologi, 44, 150-166.

Azmi, F., Basak, A. K., Adenan, M. S., Haruman, E., & Saedon, J. B. (2022). Responses of hybrid S phase layer to nanoscratching. Surface and Coatings Technology, 441, 128509.

Cabibbo, M., & Spigarelli, S. (2013). A calibration round-robin protocol for nanoindentation measurements of thin film coatings. Physics Procedia, 40, 1-8.

Chabak, Y., Efremenko, B., Petryshynets, I., Efremenko, V., Lekatou, A. G., Zurnadzhy, V., & Pastukhova, T. (2021). Structural and tribological assessment of biomedical 316 stainless steel subjected to pulsed-plasma surface modification: Comparison of LPBF 3D printing and conventional fabrication. Materials, 14(24), 7671.

Chang, X., Renqing, D., Liao, L., Zhu, P., Lin, B., Huang, Y., & Luo, S. (2023). Study on hydrodynamic lubrication and friction reduction performance of spur gear with groove texture. Tribology International, 177, 107978.

Chen, P., Jin, K., Liu, X., Qiao, X., & Yang, W. (2025). Tribological performance of textured 316L stainless steel prepared by selective laser melting. Journal of Materials Engineering and Performance, 34(1), 461-472.

Cisquini, P., Ramos, S. V., Viana, P. R. P., Lins, V. D. F. C., Franco Jr, A. R., & Vieira, E. A. (2019). Effect of the roughness produced by plasma nitrocarburizing on corrosion resistance of AISI 304 austenitic stainless steel. Journal of Materials Research and Technology, 8(2), 1897-1906.

Elhadi, A., Bouchoucha, A., Jomaa, W., Zedan, Y., Schmitt, T., & Bocher, P. (2016). Study of surface wear and damage induced by dry sliding of tempered AISI 4140 steel against hardened AISI 1055 steel. Tribology in Industry, 38(4), 475-485.

Feng, Y., Wang, H., Zhao, Z., Chen, D., Peng, Y., Gong, J., & Somers, M. A. (2024). Response of laser powder bed fusion manufactured austenitic stainless steel towards combined heat treatment and low-temperature thermochemical surface strengthening. Journal of Materials Research and Technology, 33, 1558-1568.

Ho, Y. H., Mazumder, S., Pantawane, M. V., & Dahotre, N. B. (2022). Effect of spatially varying thermokinetics on the electrochemical response of laser additively manufactured Ti6Al4V. Advanced Engineering Materials, 24(4), 2100938.

Hossain, I., Sakib Khan, M., Khan, I. K., Hossain, K. R., He, Y., & Wang, X. (2024). Technology of additive manufacturing: A comprehensive review. Kufa Journal of Engineering, 15(1).

Ibrahim, M. S., Sulaiman, M. H., & Ismail, M. I. S. (2025). Influence of oil-based and water-based lubrication on tool wear of DLC/TiAlN-coated punches in blanking of stainless steel. Jurnal Tribologi, 44, 137-149.

Jeyakymar, M., Munusami, V., Shanmugam, P., Boopalan, N., Boopathi, S., & Sureshkumar, M. (2022). An investigation on wear loss and hardness of nitro-carburizing coated stainless-steel grade-316. Materials Today: Proceedings, 66, 1398-1404.

Juri, A. Z., Azmi, F., Basak, A. K., Ghani, J. A., Kasim, M. S., & Alias, R. (2023). Tribological and corrosion behaviour of medical grade 316LVM steel by low temperature hybrid gaseous nitriding and carburizing. Tribology International, 190, 109026.

Kong, D., Dong, C., Ni, X., Zhang, L., Luo, H., Li, R., & Li, X. (2020). The passivity of selective laser melted 316L stainless steel. Applied Surface Science, 504, 144495.

Krakhmalev, P., Fredriksson, G., Svensson, K., Yadroitsev, I., Yadroitsava, I., Thuvander, M., & Peng, R. (2018). Microstructure, solidification texture, and thermal stability of 316L stainless steel manufactured by laser powder bed fusion. Metals, 8(8), 643.

Kurdi, A., Degnah, A., Juri, A. Z., Ghani, J. A., & Basak, A. K. (2024). Deformation behavior of the hybrid S-phase layer formed on a stainless-steel substrate by thermochemical heat treatment under mechanical loading. Materials Science and Engineering: A, 900, 146462.

Li, G. J., Peng, Q., Li, C., Wang, Y., Gao, J., Chen, S. Y., & Shen, B. L. (2008). Effect of DC plasma nitriding temperature on microstructure and dry-sliding wear properties of 316L stainless steel. Surface and Coatings Technology, 202(12), 2749-2754.

López-Ojeda, L., & Vargas-Gutiérrez, G. (2022). High wear resistance and better pitting corrosion resistance of AISI 316L stainless steel by a self-protective oxy-nitrocarburizing paste. Journal of Materials Research and Technology, 16, 1803-1813.

Mahmood, M. A., Chioibasu, D., Ur Rehman, A., Mihai, S., & Popescu, A. C. (2022). Post-processing techniques to enhance the quality of metallic parts produced by additive manufacturing. Metals, 12(1), 77.

Manhabosco, T. M., Muller, I. L., & Santos, C. B. D. (2009). Tribocorrosion of Ti6Al4V alloy in phosphate buffered saline solution. Química Nova, 32, 2263-2267.

Minasyan, T., Aydinyan, S., Toyserkani, E., & Hussainova, I. (2020). Parametric study on in situ laser powder bed fusion of Mo(Si1−x,Alx)2. Materials, 13(21), 4849.

Pinedo, C. E., & Tschiptschin, A. P. (2011). Low temperature nitriding, nitrocarburising and carburising of AISI 316L austenitic stainless steel. International Heat Treatment and Surface Engineering, 5(2), 73-77.

Qi, J., Guan, D., Nutter, J., Wang, B., & Rainforth, W. M. (2022). Insights into tribofilm formation on Ti-6V-4Al in a bioactive environment: Correlation between surface modification and micro-mechanical properties. Acta Biomaterialia, 141, 466-480.

Rahmatian, B., Ghasemi, H. M., Sohi, M. H., & De Baets, P. (2023). Insight into tribocorrosion resistance and tribofilm formation on titanium boride coatings in a phosphate buffer saline solution. Journal of Materials Research and Technology, 27, 6847-6862.

Renishaw plc. (2024). Stainless steel 316L (1.4404) RenAM 500 series material data sheet (H-5800-6796-03-A). Wotton-under-Edge, UK: Renishaw plc.

Rufaqua, R., Vrbka, M., Hemzal, D., Choudhury, D., Rebenda, D., Křupka, I., & Hartl, M. (2021). Analysis of chemisorbed tribo-film for ceramic-on-ceramic hip joint prostheses by Raman spectroscopy. Journal of Functional Biomaterials, 12(2), 29.

Shen, Z., Wang, F., Chen, Z., Ruan, X., Zeng, H., Wang, J., & Fan, X. (2021). Numerical simulation of lubrication performance on chevron textured surface under hydrodynamic lubrication. Tribology International, 154, 106704.

Sohif, H. N., Sulaiman, W. M. Z. W., Manshor, H., Azhar, A. Z. A., & Sukindar, N. A. (2025). Experimental investigation on surface roughness, hardness and tensile strength of rice husk (RH) as a filler for formulation of polyethylene-terephthalate glycol (PETG) 3D filament. Semarak International Journal of Material Research, 2(1), 1-11.

Tang, M., Pistorius, P. C., & Beuth, J. L. (2017). Prediction of lack-of-fusion porosity for powder bed fusion. Additive Manufacturing, 14, 39-48.

Thompson, M. K., Moroni, G., Vaneker, T., Fadel, G., Campbell, R. I., Gibson, I., & Martina, F. (2016). Design for additive manufacturing: Trends, opportunities, considerations, and constraints. CIRP Annals, 65(2), 737-760.

Wang, Y., Zhu, H., Xiao, M., Chen, C., Qi, Y., & Ke, L. (2024). Residual deformation analysis of laser powder bed fusion-fabricated lattice structures. Virtual and Physical Prototyping, 19(1), e2367104.

Wu, H. X., Ho, J. K., Dong, G. N., & Zhang, D. Y. (2015). Friction reduction of pre-phosphating nanofilm on bearing steel by tricresyl phosphate pretreatment in boundary lubrication. Proceedings of the Institution of Mechanical Engineers, Part J: Journal of Engineering Tribology, 229(1), 101-111.

Xue, Y., Zhai, L., Xu, Y., Wu, W., Jiang, Y., & Gong, J. (2025). Low-temperature nitrocarburized 316L stainless steel: Residual stress and mechanical properties. Surfaces and Interfaces, 62, 106247.

Zainal, S. U., Haruman, E., & Adenan, M. (2019). S-Phase layer development on 316 LVM using low temperature hybrid thermochemical treatment process. Journal of Mechanical Engineering (or corresponding conference proceedings).

Zhang, J., & Li, B. (2022). The influence of laser powder bed fusion (L-PBF) process parameters on 3D-printed quality and stress-strain behavior of high-entropy alloy (HEA) rod-lattices. Metals, 12(12), 2109.

Zhang, X., Liu, Y., Ma, Z., Chen,S., Ma, M., Yang, D., & Wu, Z. (2025). High-loading 316L stainless steel by integrated low-temperature surface nitriding and DLC deposition. Surface and Coatings Technology, 496, 131716.